ACS APPLIED MATERIALS & INTERFACES

Research Article

www.acsami.org

Polypyrrole Nanorod Networks/Carbon Nanoparticles Composite Counter Electrodes for High-Efficiency Dye-Sensitized Solar Cells

Shengjie Peng,*[,†,‡] Lingling Tian,[§] Jing Liang,[⊥] Subodh G. Mhaisalkar,[†] and Seeram Ramakrishna*[,#,∥]

[†] School of Materials Science and Engineering, Nanyang Technological University, 50 Nanyang Avenue, Singapore 639798

[⊥] Key Laboratory of Advanced Energy Materials Chemistry, Ministry of Education; Chemistry College, Nankai University, Tianjin, China 300071

[‡]NUS Nanoscience and Nanotechnology Initiative(NUSNNI)-NanoCore and [#]Mechanical Engineering, National University of Singapore, Singapore 117576

[§]College of Textiles, Donghua University, Shanghai, China, 201620

[∥]King Saud University, Riyadh 11451, Kingdom of Saudi Arabia

Supporting Information

ABSTRACT: Polypyrrole(PPy) nanorod networks with a high electrical conductivity of 40 S cm^{-1} have been obtained in a high yield by employing an ion association of heparin–methylene blue as a new morphology-directing agent. The polypyrrole nanorod networks are mixed with different content of carbon nanoparticles to make PPy nanorod networks/carbon nanoparticles(PPy/C) counter electrodes. It is found that the PPy/C composite with 10% carbon content shows a lower charge transfer resistance and better catalytic performance for the reduction of I_3^-, compared with the pristine PPy and carbon electrodes. The better catalytic performance is attributed to the interaction of the superior electrocatalytic activity of the unique polypyrrole nanorod networks and the carbon nanoparticles, which can accelerate triiodide reduction and electron transfer in the electrode. Under standard AM 1.5 sunlight illumination, the dye-sensitized solar cell based on the PPy/C composite with 10% carbon content as the counter electrode demonstrates a high efficiency of 7.2%, which is much higher than that of pristine PPy and carbon electrode-based DSCs and comparable to that of the thermal decomposed Pt-based DSC.

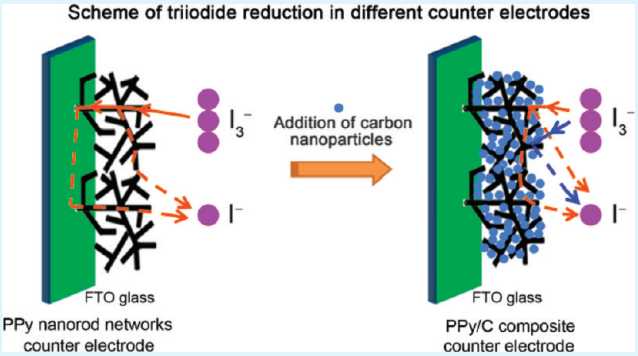

KEYWORDS: *polypyrrole nanorods, carbon nanoparticles, PPy nanorods/carbon nanoparticles electrocatalytic activity, counter electrodes, dye-sensitized solar cells*

1. INTRODUCTION

Dye-sensitized solar cells (DSCs), a special type of photoelectrochemical solar cells, have received much attention because of their low cost and simple preparation process that will be easy and affordable to manufacture.[1] Nowadays, the efficiency of the DSC can exceed 11%, which makes it promising in commercialization.[2] In the DSC, the counter electrode(CE) is one of the most important components. The role of the CE is to reduce the redox species(I_3^-/I^-) used as a mediator in regenerating the sensitizer after electron injection, and serve to transfer electrons from the external circuit back to the redox electrolyte. Therefore, an effective CE must possess high conductivity and good catalysis, which can facilitate to move electrons from within the semiconductor into an electrode and decrease the overvoltage for reduction of the redox couple.[3] Up to now, platinum is a preferred CE material due to its excellent conductivity and catalytic property for triiodide reduction. Although the necessary Pt loading for the DSCs is 5 $\mu g\ cm^{-2}$ and can not significantly contribute to the overall price of DSCs, industrial production will need abundant Pt on the earth.[3] Moreover, a small content of Pt might dissolve in triiodide-containing solutions generating platinum iodides such as PtI_4 or H_2PtI_6, which may affect the performance of DSCs.[4]

Therefore, researchers are targeting the work on developing alternative cheap materials for the counter electrodes with high conductivity, stability and efficient catalytic activity. It has been reported that some conductive polymers, carbon materials, and semiconducting materials are suitable materials for counter electrodes.[5−11] These materials showed comparable catalytic performances for triiodide reduction to the platinum electrode. Among these materials, conductive polymers are most promising candidates for CE materials due to their unique properties including low cost, high conductivity, good stability,

Received: October 23, 2011
Accepted: December 14, 2011
Published: December 14, 2011

and superior catalytic activity. Compared with the most studied polyaniline and poly(3,4-ethyl-enedioxythiophene) counter electrodes, there are only a few reports on the application of PPy as CE materials in DSCs, although PPy has been demonstrated one of the most promising candidates in the application of optical, electrical devices and sensors because of its high conductivity, environmental stability, and the virtue of easy preparation in a high yield.[12−14] With the rapid development of the nanotechnology, nanostructured conductive polymers have attracted increased attention.[5,6,15] Considering a well-ordered polymer chain structure with a large surface to volume ratio and metal-like conductivity, one-dimensional PPy has been synthesized by using "hard" templates and "soft" templates for different promising applications.[16,17] In particular, PPy with a nanostructured fibrous network is expected to provide a high electron transportation pathway for the rapid collection of photogenerated electrons and, therefore, reduce the number of interparticle hops.[18,19] Inspired by the latest findings based on the PPy with the one-dimensional network structure, we attempt to use the PPy nanorod networks as efficient CE materials for the fabrication of DSCs.

In the present study, we prepared CE materials by coating FTO glass substrates with a mixture composed of PPy nanorod networks with a high conductivity of 40 S cm^{-1} and different content of commercially available carbon nanoparticles (black pearl 1300). The carbon nanoparticles in the PPy PPy/C composite electrode can prevent the formation of relatively large open pores among the PPy nanorods, which can not only facilitate the formation of films on FTO glass but also accelerate the electron transfer in the electrode. A reason for choosing of black pearl 1300 as the additive is that such carbon black material is one of the most used carbon materials because it possesses unique properties of cheap industrial mass production, high surface area, and superior conductivity. In addition, the carbon nanoparticles having low crystallinity and many edges may be more active than highly orientated carbon materials such as graphite and carbon nanotubes.[20,21] By adjusting the carbon pearl content in the composite, the DSC based on the PPy/C composite with 10% carbon content as the counter electrode shows a high conversion efficiency of 7.2% under standard AM 1.5 sunlight illumination, which is much higher than that of pristine Ppy and carbon nanoparticle CE-based DSC, indicating a promising CE candidate for DSCs.

2. EXPERIMENTAL SECTION

2.1. Materials. Ferric chloride ($FeCl_3$), heparin, methylene blue, 4-*tert*-butylpyridine (TBP), 1,2-dimethyl-3-propylimidazolium iodide (DMPImI), lithium iodide (LiI), iodine (I_2), ethylene cellulose, titanium tetrachloride ($TiCl_4$), acetonitrile and Triton X-100 solution (~10% H_2O) were purchased from Sigma-Aldrich. Pyrrole monomer was distilled under reduced pressure before use. Carbon black pearl 1300 was obtained from Cabot Corporation. Fluorine-doped tin oxide(FTO, 7 Ω sq^{-1}, 2.2 mm thick) glass and *cis*-dithiocyanato bis(2,2′-bipyridine-4,4′-dicarboxylate)ruthenium-(II) sensitizer (N3) were obtained from Solaronix. Commercial TiO_2 (P25, a mixture of 30% rutile and 70% anatase) was obtained from Degussa AG, Germany.

2.2. Synthesis of PPy Nanorod Networks. PPy nanorod networks were synthesized by an easy chemical polymerization method.[22] In a typical synthesis, 50 mg of heparin and 100 mg of methylene blue were mixed in 50 mL of distilled water, and the PH value of the individual solution was adjusted to be 1 by using 1 M of HCl aqueous solution. Then the heparin solution and 10 mmol of pyrrole were dropped into the methylene blue solution sequentially. At last, 50 mL of 20 mM $FeCl_3$ aqueous solution was dropwisely added into the above mixture solution under a static condition, and the reaction was allowed to proceed for 12 h at room temperature. The resulting product was filtered and washed with deionized water and ethanol repeatedly. The final black product was dried by infrared dehydration.

2.3. Preparation of Counter Electrodes. The composite counter electrodes were composed of PPy nanorod networks and different content of carbon nanoparticles. It was noted that the carbon nanoparticles was commercially available as black pearl 1300 and the content of the carbon nanoparticles in the composite was based on the weight of PPy. The carbon nanoparticles were used as an additive not only to connect PPy nanorod networks together but also to bind the PPy catalyst layer to the FTO glass. The preparation of PPy/C composite with 10% content was as follows. First, 10 mg of carbon particles was dispersed in the 5 mL of Triton X-100 solution (~10% H_2O) under ultrasonic irradiation for 30 min. Then 100 mg of the obtained PPy nanorod networks was added into the mixed solution and was subjected to ultrasonic irradiation for 1 h at ambient temperature to form PPy/C electrode slurry. The PPy/C paste was coated on FTO glass by a doctor-blade method. The thickness of the films could be controlled by repeating the doctor-blade deposition. Finally, the films were dried in a vacuum oven at 150 °C for 1 h and then to be used as the counter electrode. For comparison purpose, pristine PPy, carbon, and PPy/C with other percentages of carbon nanparticles were obtained by the similar procedure. Pt electrodes were obtained by thermal decomposition. For simplification, the PPy/carbon films with 5, 10, and 15% carbon content were represented as PPy/C(5%), PPy/C(10%), and PPy/C(15%).

2.4. Preparation of Mesoporous TiO_2 Electrodes. Preparation of mesoporous TiO_2 films followed a previously described method, which was combined by screen-printing and doctor blade processes.[23,24] The FTO glass substrates were washed with basic solution, diluted nitric acid, ethanol, and acetone successively under supersonication for 30 min each before use. The preparation of TiO_2 electrodes was as follows. First, the cleaned FTO conductive glass was treated with 50 mM $TiCl_4$ aqueous solution at 70 °C for 30 min. The commercial TiO_2 paste consisting of 16.2% P25 and 4.5% ethylene cellulose in terpineol was printed on FTO conductive glass by a screen printing process for two times and then a doctor blade process. The thickness of the films could be controlled by repetition of printing. The films were dried in air at 120 °C for 30 min and calcined at 450 °C for 30 min under flowing oxygen before cooling to room temperature. Then the heated electrodes were impregnated with a 50 mM $TiCl_4$ aqueous solution in a water-saturated desiccator at 70 °C for 30 min and then recalcined at 450 °C for 30 min. When it cooled down to 80 °C, the TiO_2 films with an area of 0.16 cm^2 were soaked in a dye solution containing N3 sensitizer in a 1:1 volume mixture of acetonitrile and *tert*-butyl alcohol for 24 h at room temperature. The dye-sensitized samples were then washed in ethanol to remove unanchored dye and dried under vacuum.

2.5. Assembly of DSCs. Acetonitrile solution containing 0.1 M lithium iodide, 0.05 M iodine, 0.5 M 4-*tert*-butylpyridine, and 0.6 M 1,2-dimethyl-3-propylimidazolium iodide(DMPImI) was used as the electrolyte. DSCs were fabricated by sealing the electrolyte between the TiO_2 electrodes and the counter electrodes with a 50 μm spacer. Schematic illustration of the procedure to synthesize PPy nanorod networks and PPy/C CE is shown in Figure 1.

2.6. Characterization of Counter Electrodes and DSCs. The morphologies of the products were observed by using JEOL JSM-6700F field emission scanning electron microscope(FESEM) at an acceleration voltage of 10 kV. Fourier transform infrared(FTIR) spectroscopy of samples was recorded on a Nicolet Nexus 470 spectrometer using KBr pellets. Conductivity of the samples was tested by the four-point probe technique with a Keithley 2400 Source Meter. The surface area of the samples was detected by Brunauer−Emmett−Teller(BET) nitrogen adsorption−desorption measurement-(BELSORP-mini analyzer). Electrochemical impedance spectroscopy-(EIS) of the counter electrodes was investigated by using the Autolab PGSTAT30 from 40 Hz to 1 M Hz with signal amplitude of 10 mV to

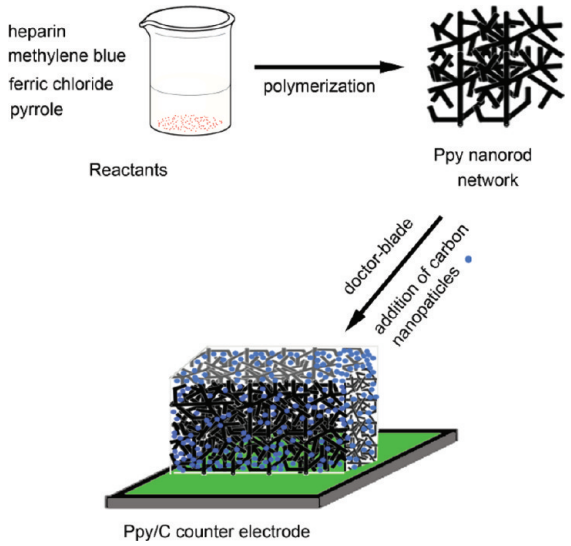

Figure 1. Schematic illustration of the procedure used to synthesize PPy nanorod networks and PPy/C counter electrode.

determine their catalytic performance. For the EIS measurement, a symmetric cell configuration with two identical counter electrodes was assembled with the injection of the same electrolyte for the DSCs, and the active area of the cells is 0.25 cm^2. EIS spectra were obtained at zero bias potential and 10 mV amplitude over the frequency range 0.01−10^5 Hz. The current density−voltage (J−V) curves of the assembled DSCs were performed using a solar simulator(San Ei, Japan) under 1 sun and at AM1.5G condition. The level of standard irradiance(1 Sun conditions, 100 mW cm^{-2}) was set with a calibrated c-Si reference solar cell.

3. RESULTS AND DISCUSSIONS

By applying the ion association of heparin−methylene blue as a template, we have successfully obtained PPy nanorod networks in a high yield(90%). The structural analysis of the obtained PPy nanorod networks was done by FTIR. Figure 2 shows the

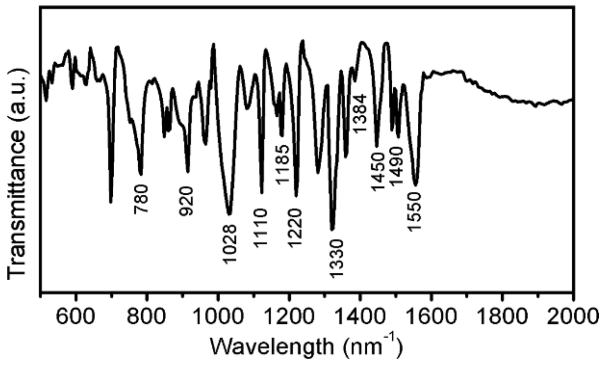

Figure 2. IR spectrum of the PPy powder.

FTIR spectrum of the PPy nanorod networks in the region of 500−2000 cm^{-1}. The peaks located at 1550, 1450, 1330, 1110, and 780 cm^{-1} are attributed to the characteristic asymmetry and symmetry stretching of pyrrole ring, stretching of C−N, vibration of C−H.[25] The band at 1384 cm^{-1} corresponding to respective stretching of N−O of heparin confirms the doping action of heparin. The FTIR spectrum also exhibits strong peaks in the region 1100−1250 and at 920 cm^{-1}, which are indicative of doped state of PPy and as such confirm the incorporation of doped ions into the grown polymer nanostructures.[25,26] It is found that methylene blue could be washed away easily by water and ethanol, because of no sign of the dye in the spectrum. As the ratio of integral intensity of absorption at 1550 and 1490 cm^{-1} is considered to reflect the criteria of effective conjugate chain of length of PPy, the obtained PPy nanorod networks possess a long effective conjugate chain, indicating a high electrical conductivity.

Figure 3a−c show the SEM and TEM images of the obtained PPy sample. It can be observed that these nanorods

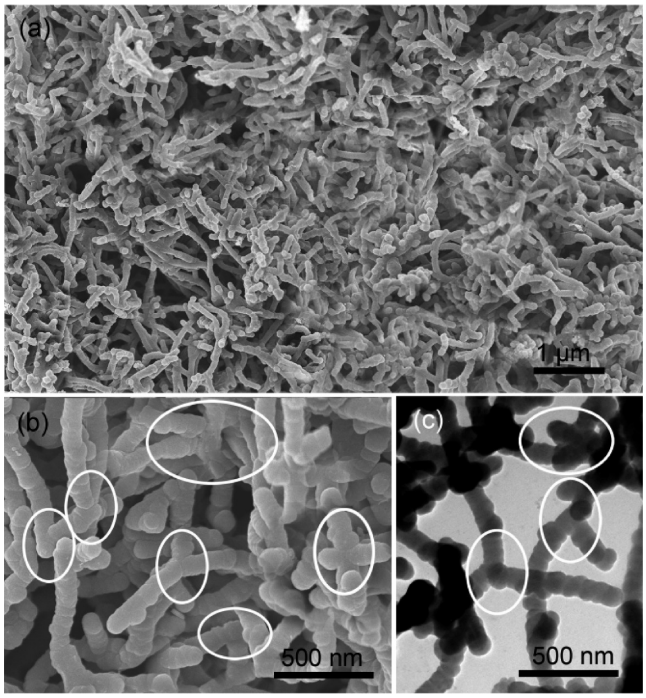

Figure 3. (a, b) SEM and (c) TEM images of the PPy powder.

interconnect with each other through some nanoparticles as "cross-linking points" (pointed out in Figure 2b,c) to form three-dimensional porous networks but not just packed structures. As PPy nanorods are not formed in the same plane, not all the "cross-linking points" of the nanorods can be clearly observed. Additionally, since the nanorods are packed densely, only those ones existing on the fringe can be clearly observed by SEM and TEM. The TEM image shows that the PPy network structure presents uniform nanorods with lengths in several micrometers and diameter of about 100 nm. The nanorod networks characteristic of PPy facilitates the electron transfer and the conductivity can reach 40 S cm^{-1}, which is higher than the random nanorods.[22] The higher electrical conductivity may be ascribed to the connected structure of PPy networks that counteract the influence of insulated cavities, leading to a relatively high conductivity.

After mixing the PPy nanorod networks with carbon nanoparticles, the obtained PPy/C composite was coated on FTO glass to investigate the effect of the different content of carbon nanaparticles on the morphologies and catalytic performance of the composite films. Figure 4a−f show SEM images of the PPy/C composite films with different carbon nanoparticles content. When the addition of carbon nanoparticles content is 10%, it can be observed that PPy nanorod networks mix well with carbon nanoparticles (Figure 4a). The magnified SEM in Figure 4b shows that PPy nanorod networks

dx.doi.org/10.1021/am201461c | ACS Appl. Mater. Interfaces 2012, 4, 397−404

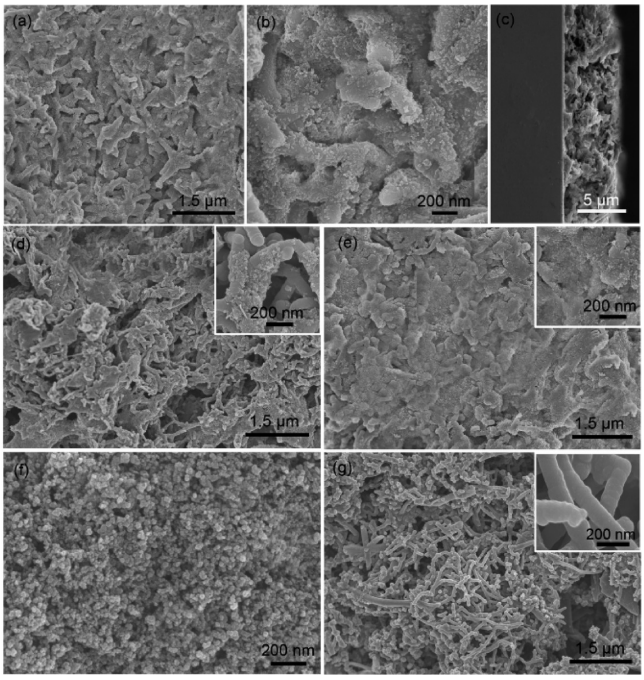

Figure 4. SEM images of the PPy/C composite films with different content of carbon nanoparticles: (a–c) 10, (d) 5, and (e) 15%, and (f) the pristine carbon and PPy(g) film electrodes. The insets are their magnified parts.

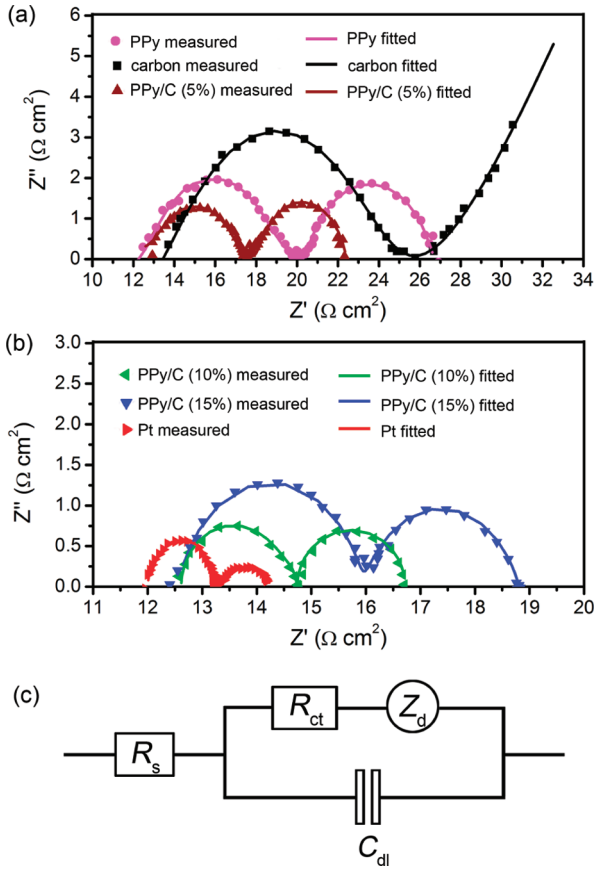

Figure 5. Nyquist plots of the symmetrical cells consisting of (a) two identical pristine PPy, carbon, Pt, and PPy/C(5%); (b) PPy/C(10%), PPy/C(15%), and Pt electrodes; and (c) the equivalent circuit for the impedance spectrum.

are coated by carbon nanoparticles with a size of 10 nm. These carbon nanoparticles fill in the voids among the PPy nanorod networks and connect PPy nanorod networks, which can be in favor of electron transfer in the film. The cross-sectional SEM image of the PPy/C composite film reveals that a uniform composite film with a thickness of 6 μm is deposited on the FTO substrate by using the doctor-blade method (Figure 4c). When the content of carbon nanoparticles decreases to 5%, some carbon nanoparticles disperse on the surface of PPy nanorods and there are some large void spaces in the film (Figure 4d). With the carbon nanoparticles content increasing to 15%, some carbon nanoparticles aggregate together easily to form a more compact film than that with less content of carbon nanoparticles and less void spaces are in the film (Figure 4e). The pristine carbon nanoparticles can form a uniform film, and there are a lot of large void spaces in the film composed of prinstine PPy nanorods networks (Figure 4f,g).

EIS measurement was conducted to analyze the electrochemical characteristics of the different counter electrodes. It can be seen that the Nyquist plots shown in Figure 5c include several regions from the high frequency regions to the low frequency regions representing various resistances: (i) ohmic serial resistance (R_s), representing the outside circuit resistance-(substrates resistance and lead connections); (ii) charge-transfer resistance (R_{ct}), corresponding to the electron transfer ability at the electrode/electrolyte interface; (iii) electrical double-layer capacitance (C_{dl}); and (iv) diffusion impedance (Z_w) of the triiodide/iodide redox couple in the electrolyte.[27,28] Table 1 summarizes the impedance parameters of various electrodes obtained by fitting the experimental data with the equivalent circuit in Figure 5. It can be seen that the R_s values of the different PPy-based counter electrodes have small R_s ranging of 12–14 Ω cm^2, indicating that a high electrical conductivity and firm bonding with the substrates.[27] These R_s

Table 1. Sheet Resistance Values and Fitted EIS Parameters of PPy, Carbon, PPy/C(5, 10, and 15%), and Pt Electrodes[a]

sample	sheet resistance (Ω γ^{-1})	R_s (Ω cm^2)	R_{ct} (Ω cm^2)	C_{dl} (μF cm^{-2})	β	Z_w (Ω cm^2)
PPy	68.32	12.29	7.81	15.32	0.89	18.93
carbon	152.01	13.70	11.10	25.21	0.88	7.55
PPy/carbon(5%)	76.32	12.42	4.82	27.05	0.87	4.81
PPy/carbon(10%)	85.40	12.51	2.32	31.31	0.84	1.72
PPy/carbon(15%)	98.12	12.56	3.99	28.80	0.86	3.32
Pt	10.18	12.15	1.20	8.64	0.94	0.93

[a]BET (Brunauer–Emmett–Teller) surface area.

values are a little larger than that of the sputtered Pt film, due to the thicker PPy-based films than Pt film.[29] The larger R_s of carbon electrode is attributed to the lower electrical conductivity (0.34 S cm^{-1}). It is known that R_{ct} is the most important part to demonstrate the catalytic ability of the counter electrodes. It is found the R_{ct} decreases with the increase of the carbon nanoparticle content in the PPy/C composite. When the content of the carbon is 10%, the R_{ct} is 2.32 Ω cm^2 and apparently lower than that of the pristine PPy and carbon electrodes, indicating higher catalytic activity than their pristine counterparts. It means that the addition of carbon nanparticles leads to the decrease of R_{ct} of the counter

dx.doi.org/10.1021/am201461c | ACS Appl. Mater. Interfaces 2012, 4, 397–404

electrodes. After adding certain carbon naoparticles, they fill in the void spaces of the PPy nanorod networks and render to better contacts among PPy matrix and I_3^- electrolytes. Such interaction can accelerate the efficient reduction reaction in the I_3^-/I^- system and lead to the improvement of the catalytic activity. Also the carbon nanoparticles have some catalytic activity for the I_3^- reduction. The schematic diagram of the triiodide reduction by the pristine PPy and PPy/C composite counter electrodes is shown in Figure 6. If the carbon content

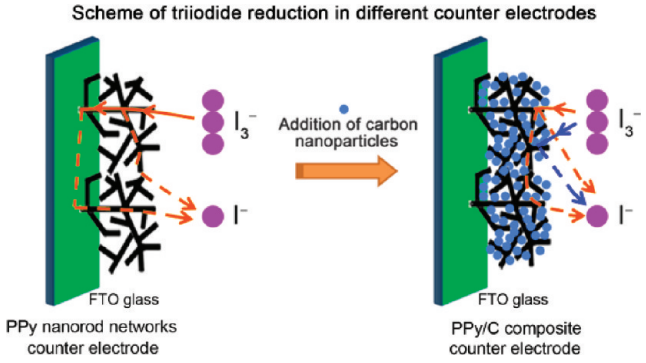

Figure 6. Schematic diagram of triiodide reduction on the pristine PPy nanorod networks and PPy/C composite counter electrodes, respectively.

increases to 15%, the R_{ct} of the composite instead increase to 3.99 Ω cm^2. One possible reason is the more carbon nanoparticles not only disperse in PPy matrix but also aggregate on the surface PPy/C, indicated by the SEM image, which block the contact between PPy matrix and I_3^- electrolyte.[9]

It is reported that impedance of the CE/electrolyte interface deviates a little from the ideal capacitance; therefore, more accurate analysis shows that the capacitance should be replaced by a constant phase element (CPE).[20] The impedance Z_{CPE} of a CPE is described as $Z_{CPE} = B(i\omega)^{-\beta}$ $(0 \le \beta \le 1)$, B and β are frequency-independent parameters of the CPE. If β is 1, the CPE shows a perfect capacitor, exhibiting an exact semicircle in the Nyquist plots.[29] In the case of β less than 1, the semicircle is depressed, due to the porosity of the electrode surface. It is found that the PPy/C(10%) presents the smallest β among the various Pt-free counter electrodes. It should be noted that the β values of carbon and PPy/C(15%) are higher than that of PPy/C(10%), although the measured BET and the total pore volume values of the carbon and PPy/C(15%) are higher than those of PPy/C(10%) (Table S1 in the Supporting Information). This could be attributed to the limited accessibility of electrolyte into the internal active surface of carbon and PPy/C(15%) electrodes.[30] This can also explain the increased Z_w of the carbon and PPy/C(15%). The smaller Z_w of PPy/C(10%) indicates a faster diffusion velocity of the redox couple in the electrolyte than that of PPy, carbon, PPy/C(5%) and PPy/C(15%) films.

CV characterization is another important and efficient tool to analyze the relationship between ion diffusivity and the catalytic mechanism acting in an electrochemical system. Figure 7 shows the CV curves of pristine PPy, carbon, PPy/C, and Pt electrodes for I^-/I_3^- redox system (versus Ag/AgCl) in 10 mM LiI, 1 mM I_2 acetonitrile solution containing 0.1 M $LiClO_4$ as the supporting electrolyte. Two typical pairs of oxidation/reduction peaks were observed for the various counter electrodes and the corresponding reactions are

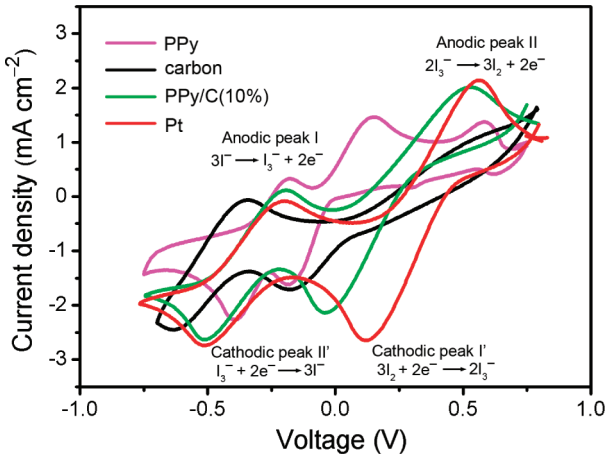

Figure 7. Cyclic voltammograms of pristine PPy, carbon, PPy/C(10%), Pt electrodes at a scan rate of 50 mV s^{-1} in 10 mM LiI, 1 mM I_2 acetonictrile solution containing 0.1 M $LiClO_4$ as the supporting electrolyte.

shown in Figure 7. In a DSC, the photoexcited electrons from the dye are injected into the TiO_2 conduction band. Then the oxidized dye is reduced by the I^- ion in the electrolyte, and the resulting I_3^- ion are reduced at the CE. Therefore, the research focus is the characteristics of the left pair of peak, which is attributed to the reaction of $I_3^- + 2e^- = 3I^-$.[6,31] The oxidation and reduction peaks observed in the PPy/C are comparable to those of the Pt electrode, indicating the possibility of achieving similar electrocatalytic activity, as a high redox current density of the CE implies a high electrocatalytic activity for I_3^- reduction at this CE. It is found that pristine PPy and carbon electrodes show a much lower current density, indicating a poor reduction rate compared to PPy/C and Pt electrodes. Moreover, the higher redox current density describes the stronger electrocatalytic activity toward the reduction of I_2 to I_3^- ions and increases the reduction of the I_3^- ions to I^- ions in the redox couple at the counter electrode.[32] This result coincides with the charge transfer resistance R_{ct} obtained from the EIS measurements. A possible reason of the higher electrocatalytic activity in the PPy/C electrode is that carbon nanoparticles can better connect with the PPy with a unique nanorod network structure and high conductivity, which can facilitate electron transfer. Therefore, PPy/C counter electrode can be used as an efficient electrocatalyst counter electrode material in DSCs.

Figure 8 shows the $J-V$ curves of the DSCs based on pristine PPy, carbon, PPy/C(5%, 10%, and 15%) and Pt counter electrodes under AM 1.5 solar simulator illumination at 100 mW cm^{-2}. The thicknesses of all the counter electrodes are 6 μm. The photovoltaic parameters of the DSCs are summarized in Table 2. It is found that the PPy/C(10%)-based DSC exhibits a short-circuit current density (J_{sc}) of 15.2 mA cm^{-2}, open-circuit voltage (V_{oc}) of 710 mV, and fill factor (FF) of 66.8%, yielding a relatively energy conversion efficiency(η) of 7.2%. However, the pristine PPy and carbon counter electrodes reached conversion efficiency of 5.0% and 4.3%, respectively, which is much lower than that of PPy/C (10%)-based DSC. Furthermore, the efficiency of 7.2% is the highest among the free Pt-based DSCs and 92% that of the typical Pt-based DSC (7.8%), indicating that the PPy/C composite may be a promising candidate for the counter electrodes for the DSCs. Compared with photovoltaic parameters between the PPy/C

dx.doi.org/10.1021/am201461c | ACS Appl. Mater. Interfaces 2012, 4, 397–404

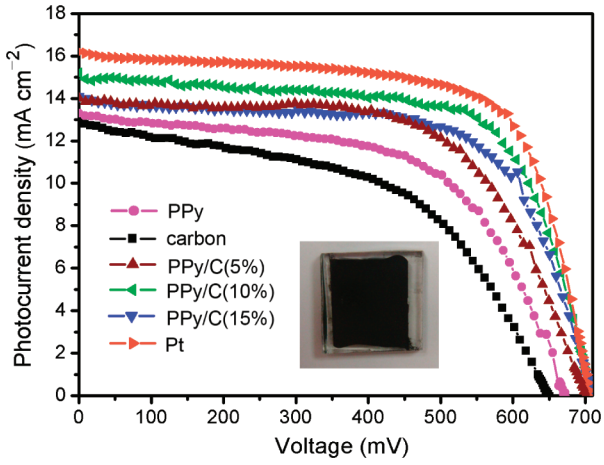

Figure 8. Current density–voltage (J–V) curves of the DSCs based on pristine PPy, carbon, PPy/C(5, 10, and 15%) and Pt counter electrodes under AM 1.5 (100 mW cm^{-2}).

Table 2. Photovoltaic Parameters of the DSCs by Using Pristine PPy, Carbon, PPy/C(5, 10, and 15%) and Pt Counter Electrodes under AM 1.5 (100 mW cm^{-2})

counter electrode	J_{sc} (mA cm^{-2})	V_{oc} (mV)	FF (%)	η (%)
PPy	13.3	680	55.5	5.0
carbon	12.9	650	51.2	4.3
PPy/carbon(5%)	14.0	702	62.1	6.1
PPy/carbon(10%)	15.2	710	66.8	7.2
PPy/carbon(15%)	14.1	713	65.1	6.5
Pt	16.2	707	68.3	7.8

CE and the pristine PPy electrodes, it is observed that the pristine one shows much lower short-circuit current density and fill factor, which leads to a poor performance. It has been demonstrated that the introduction of carbon nanoparticles in PPy matrix not only decreased the charge-transfer resistance in the electrolyte/electrode interface, but also reduced the diffusion impedance of triiodide ions, leading to the high J_{sc} and *FF* for DSCs. Meanwhile, the electron-transport network formed by PPy also plays an indispensable role in the high photovoltaic performance. It is found that the commercial carbon nanoparticles without the PPy nanorod networks exhibit a very low *FF* and a poor photovoltaic performance because of the low catalytic activity, further demonstrating the importance of PPy/C electron transport network. However, as the carbon content in the PPy/C composite increases to 15%, the conversion efficiency of the DSC decreases to 6.5%, which is lower than the PPy/C(10%)-based DSC. The possible reason is that more carbon nanoparticles can be a barrier to the contacts between efficient PPy network and I_3^-. This may reduce electron transport on the CE and the regeneration rate of dye molecules, leading to the reduced J_{sc} and FF. Despite the relatively high efficiency, the PPy/C CE device shows a little lower efficiency than that of Pt-based DSC, due to the lower FF and J_{sc}. The higher internal resistance leads to the reduced FF. Furthermore, the lower J_{sc} can be influenced not only by the internal resistance but also photoreflection properties related to the counter electrodes, due to the high photoabsorption ability of black PPy/carbon materials.[33] In a word, as the raw materials of carbon nanoparticles iares commercially available and PPy nanorod networks can be synthesized in a high yield, this PPy/carbon composite is a cost-efficient and promising CE material for DSCs.

It has been reported that the thickness of the counter electrodes can influence the performance of the DSCs.[20,34] In this work, the effect of the PPy/C(10%) composite thickness on the performance of the DSCs was also evaluated. To better understand the influence of the PPy/C(10%) composite thickness on the performance of the DSCs, we fist measure the photovoltaic performance of the pristine PPy and carbon with the thickness of 2 μm, 6 μm, 10 μm, respectively (Table S2 in the Supporting Information). The photovoltaic efficiencies of the DSCs based on the pure PPy and carbon are improved, as the thicknesses of the PPy and carbon films increase (Table S2 in the Supporting Information). It is found that the increase of J_{sc} and FF leads to improvement of the DSCs. This result can be ascribed to the increasing catalytic active surface area of the counter electrodes with the increased thickness, which leads to the increase of the J_{sc} and FF and further increase of the efficiency. With regard to the PPy/C(10%) composite film, it can be observed that the thickness of the films is about 1, 4, 10, and 16 μm by adjusting the repetition of the doctor blade process (Figure S1 in the Supporting Information). Figure 9 and Table 3 show the J–V curves of the

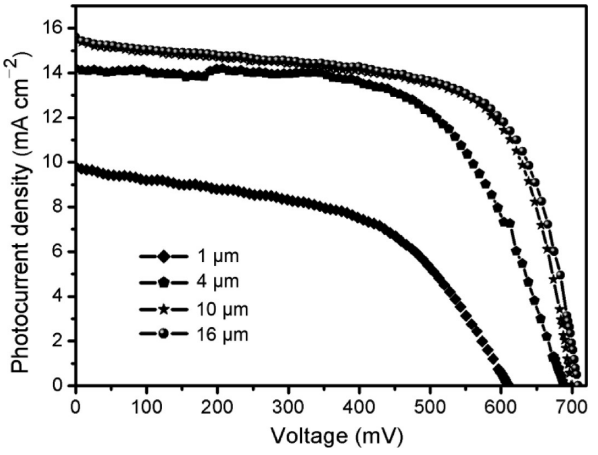

Figure 9. Cross-sectional SEM images of the PPy/C(10%) films with different thicknesses and the current density–voltage (J–V) curves of the DSCs based on such PPy/C(10%) films with different thicknesses as counter electrodes under AM 1.5 (100 mW cm^{-2}).

Table 3. R_{ct} Values of the PPy/C(10%) Films with Different Thicknesses and Photovoltaic Parameters of the DSCs Based on PPy/C(10%) Films with Different Thickness As Counter Electrodes under AM1.5 (100 mW cm^{-2})

smple thickness(μm)	R_{ct} (Ω cm^2)	J_{sc} (mA cm^{-2})	V_{oc} (mV)	*FF* (%)	η (%)
1	10.01	9.8	610	51.4	3.0
4	4.02	14.2	690	62.5	6.1
10	4.82	15.5	700	66.3	7.1
16	2.32	15.4	710	66.0	7.2

DSCs based on PPy/C(10%) counter electrodes with a thickness of 1, 4, 10, and 16 μm under AM 1.5 (100 mW cm^{-2}), respectively. It can be found that the conversion efficiency of the DSC is only 3.1%, when the PPy/C with a thickness of 1 μm was used as the counter electrode. This is attributed to the poor quality of the PPy/C film. It can be observed by naked eyes that the FTO glass substrate is not fully

covered by the PPy/C composite due to the relatively large PPy nanorod networks. This makes insufficient PPy/C composite expose to the electrolyte, leading to a low J_{sc} and FF. With the PPy/C film thickness increase to 4 μm, the conversion efficiency increases to 6.1%. To achieve higher energy conversion efficiency, the thickness of the PPy/C films is continually increased. And the efficiency of the DSC based on the 10-μm-thickness PPy/C film reaches 7.1%, which can be ascribed to the increasing catalytic active surface area of the PPy with the increased thickness. With the PPy/C film thickness further increase to 16 μm, the efficiency of the DSC is 7.2%, which is almost the same as that of DSC with a 10-μm-thickness PPy counter electrode. It can be found that the R_{ct} of PPy/C(10%) films decreases, as the thickness of the PPy/C(10%) film increases. The reduction of R_{ct} is attributed to the increase of surface area with the thick PPy/C(10%) film. The lower R_{ct} implies relatively higher exchange current density on the PPy/C(10%) electrode according to the following equation: $J_0 = RT/nFR_{ct}$, where R is the molar gas constant, T is the temperature, F is Faraday constant.[35,36] Therefore, faster reduction rate of I_3^- ions with the PPy/C(10%) electrode can lead to an increase in J_{sc}, due to the decrease R_{ct}. Compared to the Pt electrode, the decreased J_{sc} derives from not only the lower R_{ct} but also its poor photoreflection property, which is connected with its high photoabsorption ability of PPy/C(10%) materials. Further studies to understand the difference in cell performance with the different thicknesses are currently underway. Based on the performance of DSCs using PPy CEs with different thickness, it is concluded that the increase of the PPy/C film thickness can result in increase of catalytic performance and further improvement of the conversion efficiency. Furthermore, the energy conversion efficiency of DSC based on PPy/C(10%) counter electrode retained 93% of its initial value after 20 days (Figure S2 in the Supporting Information). Therefore, the DSC can reach a conversion efficiency of 7.2% with the optimized PPy/C thickness of 6 μm.

4. CONCLUSIONS

In conclusion, PPy nanorod networks have been successfully fabricated by a chemical oxidation process in a high yield and were mixed with commercially available carbon nanoparticles as efficient CE materials in DSCs. It has been demonstrated that the PPy/C with 10% carbon nanoparticle content presents good catalytic activity for the I_3^- reduction. The DSC based on such PPy/C(10%) CE reaches a conversion efficiency of 7.2%, which is better than the individual pristine PPy and carbon nanoparticle films-based DSC, and comparable to the sputtered Pt based-DSC. This is attributed to the superior electrocatalytic activity and high electrical conductivity derived from the unique PPy nanorod network structure. Furthermore, the carbon nanoparticles in the PPy/C composite can not only fill in the void spaces of the PPy nanorod networks to enhance electron transfer but also facilitate the formation of PPy/C film. Therefore, the PPy/C composite with a high photovoltaic performance is competitive with the conventional and expensive Pt CE, and a promising CE material candidate for efficient DSCs.

■ ASSOCIATED CONTENT

Supporting Information

Cross-sectional SEM images of the PPy/C(10%) films with different thicknesses, a short-term evaluation of the stability of the sealed DSC, BET surface areas and total pore volumes of different samples, photovoltaic parameters of the DSCs based on pristine PPy and carbon films with different thickness. This material is available free of charge via the Internet at http://pubs.acs.org.

■ AUTHOR INFORMATION

Corresponding Author

*E-mail: sjpeng@ntu.edu.sg(S.P.); seeram@nus.edu.sg (S.R.a).

■ ACKNOWLEDGMENTS

This work was supported by Singapore NRF-CRP grant on "Nanonets for harnessing solar energy and storage" and the National High Technology Research and Development Progress of China (2009AA03Z233).

■ REFERENCES

(1) O'Regan, B.; Grätzl, M. *Nature* **1991**, *393*, 737−740.
(2) Nazeeruddin, M. K.; Angelis, F. D.; Fantacci, S.; Selloni, A.; Viscardi, G.; Liska, P.; Ito, S.; Takeru, B.; Grätzel, M. *J. Am. Chem. Soc.* **2005**, *127*, 16835−16847.
(3) Papageorgiou, N. *Coord. Chem. Rev.* **2004**, *248*, 1421−1446.
(4) Olsen, E.; Hagen, G.; Lindquist, S. E. *Sol. Energy Mater. Sol. Cells* **2000**, *63*, 267−273.
(5) Pringle, J. M.; Armel, V.; MacFarlane, D. R. *Chem. Commun.* **2010**, *46*, 5367−5369.
(6) Tai, Q. D.; Chen, B. L.; Guo, F.; Xu, Sh.; Hu, H.; Sebo, B.; Zhao, X. Z. *ACS Nano* **2011**, *5*, 3795−3799.
(7) Wu, M. X.; Zhang, Q. Y.; Xiao, J. Q.; Ma, C. Y.; Lin, X.; Miao, C. Y.; He, Y. J.; Gao, Y. R.; Hagfeldt, A.; Ma, T. L. *J. Mater. Chem.* **2011**, *21*, 10761−10766.
(8) Sun, H. C; Qin, D.; Huang, S. Q.; Guo, X. Z.; Li, D. M.; Luo, Y. H.; Meng, Q. B. *Energy Environ. Sci.* **2011**, *4*, 2630−2637.
(9) Sudhagar, P.; Nagarajan, S.; Lee, Y. G.; Song, D.; Son, T.; Cho, W.; Heo, M.; Lee, K.; Won, J.; Kang, Y. S. *ACS Appl. Mater. Interfaces* **2011**, *3*, 1838−1843.
(10) Li, G. R.; Wang, F.; Jiang, Q. W.; Gao, X. P.; Shen, P. W. *Angew. Chem., Int. Ed.* **2010**, *49*, 3653−3656.
(11) Saito, Y.; Kitamura, T.; Wada, Y.; Yanagida, S. *Chem. Lett.* **2002**, *31*, 1060−1061.
(12) Jeon, S. S.; Kim, C.; Ko, J.; Im, S. S. *J. Mater. Chem.* **2011**, *21*, 8146−8151.
(13) Wu, J. H.; Li, Q. H.; Fan, L. Q.; Lan, Z.; Li, P. J.; Lin, J. M.; Hao, S. C. *J. Power Sources* **2008**, *181*, 172−176.
(14) Xia, J. B.; Chen, L.; Yanagida, S. *J. Mater. Chem.* **2011**, *21*, 4644−4649.
(15) Biswas, S.; Drzal, L. T. *Chem. Mater.* **2010**, *22*, 5667−5956.
(16) Zang, J. F.; Li, C. M.; Bao, S. J.; Cui, X. Q.; Bao, Q. L.; Sun, C. Q. *Macromolecules* **2008**, *41*, 7053−7056.
(17) Li, J.; Lin, X. Q. *Biosens. Bioelectron.* **2007**, *22*, 2898−2905.
(18) Zhong, W. B.; Liu, S. M.; Chen, X. H.; Wang, Y. X.; Yang, W. T. *Macromolecules* **2006**, *39*, 3224−3230.
(19) Klempner, D.; Sperling, L. H.; Utracki, L. A. Interpenetrating Polymer Networks; Advances in Chemistry Series; American Chemical Society: Washington, D.C., 1994; Vol. *239*, p 3−179.
(20) Murakami, T. N.; Ito, S.; Wang, Q.; Nazeeruddin, M. K.; Bessho, T.; Cesar, I.; Liska, P.; Humphry-Baker, R.; Comte, P.; Péchy, P.; Grätzel, M. *J. Electrochem. Soc.* **2006**, *153*, A2255−A2261.
(21) Kinoshita, K.; Carbon, Electrochemical and Physicochemical Properties; Wiley-Interscience: New York, 1987; p 226−379.
(22) Wei, M.; Dai, T. Y.; Lu, Y. *Synth. Met.* **2010**, *160*, 849−854.
(23) Peng, S. J.; Shi, J. F.; Pei, J.; Liang, Y. L.; Cheng, F. Y.; Liang, J.; Chen, J. *Nano Res.* **2009**, *2*, 484−492.
(24) Peng, S. J.; Cheng, F. Y.; Shi, J. F.; Liang, J.; Tao, Z. L.; Chen, J. *J. Solid State Sci.* **2009**, *11*, 2051−2055.
(25) Goel, S.; Mazumdar, N. A.; Gupta, A. *Polym. Adv. Technol.* **2010**, *21*, 205−210.
(26) Wei, M.; Lu, Y. *Syn. Met.* **2009**, *159*, 1061−1066.

(27) Wu, M. X.; Lin, X.; Wang, T. H.; Qiu, J. S; Ma, T. L. *Energy Environ. Sci.* **2011**, *4*, 2308−2315.
(28) Cho, S. J.; Ouyang, J. Y. *J. Phys. Chem. C* **2011**, *115*, 8519−8526.
(29) Joshi, P.; Zhang, L. F.; Chen, Q. L.; Galipeau, D.; Fong, Hao.; Qiao, Q. Q. *ACS Appl. Mater. Interfaces* **2010**, *2*, 3572−3577.
(30) Wang, G. Q.; Huang, C. C.; Xing, W.; Zhuo, S. P. *Electrochim. Acta* **2011**, *56*, 5459−5463.
(31) Ameen, S.; Akhtar, M. S.; Kim, Y. S.; Yang, O. B.; Shin, H. S. *J. Phys. Chem. C* **2010**, *114*, 4760−4764.
(32) Jia, R. R.; Chen, J. Z.; Zhao, J. H.; Zheng, J. F.; Song, C.; Li, L.; Zhu, Z. P. *J. Mater. Chem.* **2010**, *20*, 10829−10834.
(33) Veerappan, G.; Bojan, K.; Rhee, S. W. *ACS Appl. Mater. Interfaces* **2011**, *3*, 857−862.
(34) Imoto, K.; Takahashi, K.; Yamaguchi, T.; Komura, T.; Nakamura, J.; Murata, K. *Sol. Energy Mater. Sol. Cells* **2003**, *79*, 459−469.
(35) Zhang, Q. X.; Zhang, Y. D.; Huang, S. Q.; Huang, X. M.; Luo, Y. H.; Meng, Q. B.; Li, D. M. *Electrochem. Commun.* **2010**, *12*, 327−330.
(36) Wu, M. X.; Lin, X.; Wang, T. H.; Qiu, J. S.; Ma, T. L. *Energy Environ. Sci.* **2011**, *4*, 2308−2315.